

Original paper

Geochronology and characteristics of Ni–Cu–(PGE) mineralization at Rožany, Lusatian Granitoid Complex, Czech Republic

Eva HALUZOVÁ^{1,2*}, Lukáš ACKERMAN^{2,3}, Jan PAŠAVA³, Šárka JONÁŠOVÁ², Martin SVOJTKA², Tomáš HRSTKA², František VESELOVSKÝ³

¹ Faculty of Science, Charles University, Albertov 6, 128 43 Prague 2, Czech Republic; haluzova@gli.cas.cz

² Institute of Geology, The Czech Academy of Sciences, Rozvojová 269, 165 00 Prague 6, Czech Republic

³ Czech Geological Survey, Geologická 6, 152 00 Prague 5, Czech Republic

*Corresponding author



The Ni–Cu–(PGE) mineralization at Rožany is located in the northern part of the Bohemian Massif and it is hosted by gabbroic dykes (dolerites) cross-cutting the granitic Lusatian Granitoid Complex. The intrusion of dolerite is newly well constrained by *in-situ* LA–ICP–MS U–Pb zircon age of 349 ± 3 Ma (2σ), which is much younger than previous K–Ar and Pb–Pb data. The barren dolerites are characterized by high enrichments of some incompatible elements (e.g., LREE, Zr, Sr) and radiogenic Os isotopic composition suggesting their derivation from enriched (metasomatized) mantle source, possibly due to subduction processes. The mineralization itself is represented by pyrrhotite, chalcopyrite and pentlandite; the latter is commonly replaced by violarite most likely due to late-stage hydrothermal alteration. The origin and formation of at least some platinum-group minerals was probably closely associated with late-stage hydrothermal processes, causing remobilization of platinum-group elements from the primary base-metal sulphides. The Ni-rich ores exhibit the highest I-PGE (Os, Ir, Ru) concentrations whereas Pd and Pt tend to be enriched in Cu-rich ores. Observed variations in Re–Os isotopic compositions of the massive and disseminated ore types from the Rožany expressed by highly variable initial (349 Ma) γ Os values of +50 to +134 in part indicates important, but variable amounts of incorporated crustal material. However, very similar $^{187}\text{Re}/^{188}\text{Os}$ values found in all rock types can be best explained by post-crystallization Re loss associated with late-stage hydrothermal alteration. When compared to other Ni–Cu–(PGE) mineralizations in the Bohemian Massif, the total PGE contents found in Rožany are much lower than those reported from the Ransko Massif, but similar to those in the Svitavy ultramafic Complex.

Keywords: Ni–Cu–(PGE), Lusatia, Re–Os, Bohemian Massif, sulphur

Received: 16 September, 2015; **accepted:** 28 December, 2015; **handling editor:** E. Jelínek

1. Introduction

Mantle-derived mafic to ultramafic rocks (peridotites, gabbros, komatiites, basalts) represent important source of platinum-group (PGE) and chalcophile (e.g., Ni, Cu, Zn) elements (Crocket 2002; Naldrett 2010). At many places worldwide, PGE deposits are located in variable tectonic settings with common association with chromite reefs, Ni–Fe massive sulphides and/or magnetites (Naldrett 2010). The Ni–Cu–(PGE) mineralizations are predominantly connected with mafic rocks such as flood basalts (Norilsk; Naldrett 2010), komatiites (Kambalda; e.g., Leshner et al. 1984) or gabbroic cumulates within layered intrusions (Bushveld – e.g., Cawthorn et al. 2002; Sudbury – e.g., Lightfoot and Doherty 2001).

The Bohemian Massif is the easternmost and largest exposure of the Variscan orogenic belt in Europe, which is known for its numerous Au, Sn–W, U and base-metal as well as rarer Ni–Cu mineralizations located in different geotectonic units. Based on geological, mineralogical and economic geology data, more than 120 types of

ore mineralizations were described by Bernard (1991). Magmatic Ni–Cu–(PGE) ores were identified at three localities – Staré Ransko (e.g., Pokorný 1969; Pašava et al. 2003), Rožany/Kunratice (e.g., Vavříň and Frýda 1998; Pašava et al. 2001) and Svitavy (Kopecký 1992; Pašava et al. 2007).

The Ni–Cu–(PGE) mineralization at Rožany occurs in the Lusatian Granitoid Complex. It is characterized by low-grade Ni–Cu sulphide ores, which are hosted by gabbroic dykes (dolerites), but also form impregnations in the surrounding granitic rocks. In the 15th century, Rožany deposit was important source of copper, and in the 17th century it was mined for Ni. The last geological exploration in 1960s showed that contents of the Ni and Cu in ores have negative balance character. However, fairly recent discovery of platinum-group mineralization (Vavříň and Frýda 1998) indicates that the Rožany deposit could become a potential source of PGE in the future. Therefore, it is important to learn more on the character, formation and evolution of the host rocks and the PGE mineralization itself.

The ores are characterized by predominant occurrence of pyrrhotite, chalcopyrite, minor Fe–Ni sulphides (violarite, pentlandite) and rare pyrite with galena (Pašava et al. 2001). The mineralization occurs directly in the dolerite dykes and/or on the contact between dolerite and host granites. It consists of several ore types including (a) massive pyrrhotite–pentlandite ore, (b) massive pyrrhotite–chalcopyrite ore and (c) disseminated ore. Within these types, Pt–Pd–As–Te mineralization represented by unnamed Pd-bearing tellurides [$\text{Pd}_2(\text{Ni},\text{Fe})_2\text{BiTe}_6$, $\text{PdNi}(\text{Sb},\text{Bi})\text{Te}_2$], sperrylite [PtAs_2], melonite [NiTe_2] and vavřinite [SbNi_2Te_2] was described (Vavřín and Frýda 1998; Pašava et al. 2001).

In this paper, we present sulphide petrography of the massive and disseminated ores together with their chalcophile/siderophile element geochemistry and Os–S isotopic compositions. We also bring new mineralogical data on the platinum-group minerals (PGM) and on geochemistry and U–Pb zircon geochronology of the host dolerite. Based on these findings, we provide better constraints on the nature, conditions and evolution of sulphide mineralization at Rožany deposit and its temporal relationship to the host Lusatian Granitoid Complex.

2. Geological setting and samples

The Bohemian Massif formed during collision of Gondwana, Laurussia and associated microcontinents during the Late Paleozoic (e.g., Matte 2001). Four major tectonic zones can be distinguished within Bohemian Massif: the Saxothuringian, the Teplá–Barrandian, the Moldanubian and the Moravo–Silesian (Schulmann et al. 2009). The Rožany deposit is situated in the northernmost part of the Bohemian Massif, which belongs to the Saxothuringian Zone (Fig. 1). This area NE of the Elbe tectonic zone (Fig. 1) has been traditionally called the Lusatian Unit or Western Sudetes (e.g., Kosmatt 1927). It consists of Cadomian basement represented by metamorphosed Neoproterozoic sediments and granitic rocks, overlain by a Palaeozoic (Cambrian to Carboniferous) overstep sequence (Linnemann et al. 2008). The NE part of the Lusatian Unit is represented by the Lusatian Block (Fig. 1) which consists of (i) Lusatia–Leipzig Greywacke Complex associated with Torgau–Doberlug syncline, and (ii) Lusatian Granitoid Complex (Linnemann et al. 2008).

2.1. Lusatia–Leipzig Greywacke Complex

This unit is classified as Cadomian retro-arc basin characterized by monotonous, deep-marine sections of turbidites (greywacke and mudstone couplets) accompanied by conglomerates. The U–Pb geochronology of detrital zircon

grains from the Lusatia–Leipzig Greywacke Complex indicates that they are younger than 555 ± 9 Ma (Linnemann et al. 2004) with maximum age of deposition of 543 ± 4 Ma obtained for a youngest zircon generation found in the conglomerate (Linnemann et al. 2007).

2.2. Lusatian Granitoid Complex

The Lusatia–Leipzig Greywacke Complex was intruded by voluminous granitic intrusions forming the large (100×50 km) Lusatian Granitoid Complex (LGC) of ~ 590 – 500 Ma age (U–Pb zircon dating – Kröner et al. 1994; Linnemann et al. 2000; Dörr et al. 2002; Tichomirowa 2002; Białek et al. 2014). The LGC formed most likely by melting of the Lusatia–Leipzig Greywacke Complex as the granites contain abundant inherited zircons of matching age. Three main types of granitic rocks can be distinguished: (1) two-mica and biotite granodiorite (~ 590 – 550 Ma) predominantly occurring at SW part of the LGC, (2) amphibole–biotite granodiorite and monzogranite (~ 530 – 520 Ma) forming most of the central part of the LGC and (3) the Rumburk granite and its metamorphic equivalent represented by the Jizera orthogneiss (~ 500 Ma: Oberc-Dziedzic et al. 2009, 2010; Żelaźniewicz et al. 2009) forming the eastern part of the LGC.

In the Cambrian, exhumation of the LGC started with tectonic segmentation accompanied by the origin of depressions and elevations, appearance of the first faults and beginning of denudation of the whole area. The last magmatic activity in the LGC was related to Variscan orogeny. The LGC is characterized by the abundance of dykes with compositions ranging from acidic to basic. The mafic dykes (dolerites) form dyke swarm of $\sim W$ – E direction (Fig. 1) concentrated in faults or fissures; its composition varies from quartz diorite to olivine gabbro (Cháb et al. 2010). Ages of these dykes are poorly constrained with reported K–Ar and Pb–Pb ages ranging from 400 to 265 Ma (Kramer 1977; Kozdrój et al. 2001; Kindermann et al. 2003). The Rožany locality is situated in the Lipov–Rožany granodiorite with the age of 462–501 Ma (Rb–Sr geochronology; Borkowska et al. 1980) with petrogenesis similar to the Rumburk granite.

3. Analytical methods

Studied samples were collected from Rožany deposit at two old nearby quarries (location of the first quarry: N $51^\circ 2.09'$; E $14^\circ 27.08'$, of the second: N $51^\circ 2.05'$; E $14^\circ 27.87'$) during two field campaigns in 2014–2015. In total, six samples of massive ores, two samples of disseminated ores and one sample of barren dolerite (the last also for U–Pb dating) have been selected from a large sample collection.

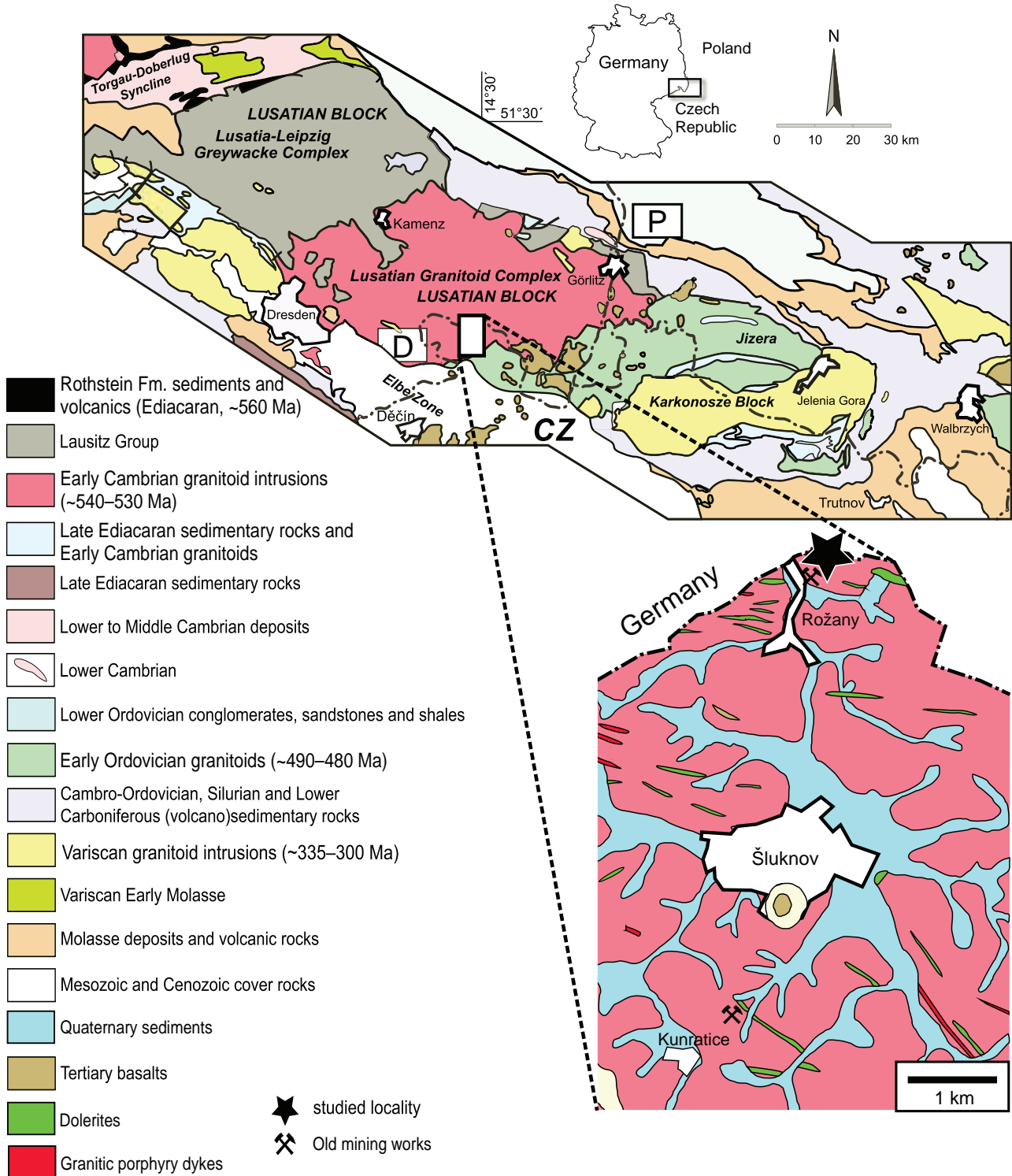


Fig. 1 Generalized geological map of the studied area in northern Bohemia (adopted and modified from Linnemann et al. 2008) with a focus on the Rožany–Kunratice area.

3.1. Trace-element analyses

Trace-element (lithophile and chalcophile elements) concentration measurements in dolerites and ore samples were carried out using an Element 2 sector field ICP-MS

(Thermo-Finnigan) housed at the Institute of Geology of the Czech Academy of Sciences (IG CAS), Prague. To prevent As loss, decomposition of sulphide-rich samples (~100 mg) was performed in Teflon vials with mixture of 3 ml HNO₃, 1 ml HCl and 1 ml HF using Micro-

wave Accelerated Decomposition System (Milestone). The residual solution was mixed with 10 ml of H_3BO_3 saturated solution and decomposed again in microwave system. The final solution was diluted for ICP–MS measurements. Calibration was carried out with an aqueous multi-element solutions (EPond, Switzerland) and ^{115}In as internal standard for correction of instrumental drift. Trace elements such as REE, Rb, Sr, Cs, Ba, Y, U, Th, Pb, Zr, Hf and Nb were measured in low ($m/\Delta m = 300$) resolution modes whereas Sb, Te, Bi, As, Se, V, Cr, Co, Ni, Zn and Cu were measured in medium ($m/\Delta m = 4000$) resolution mode. The in-run precision of the analyses was typically better than 1 % for all analysed elements. The accuracy of the trace-element analyses was checked against BCR-2 (USGS) and WMS-1 (Canmet) reference materials, respectively, yielding deviation of up to 15 % except As and Se with deviation of –20 % with respect to certified values.

3.2. Modal sulphide compositions and platinum-group minerals analyses

Modal sulphide composition in the samples was obtained by automated mineralogy approach (Gottlieb et al. 2000; Smith et al. 2013) using the TESCAN Integrated Mineral Analyser (TIMA) at the IG CAS. The analysis combined BSE and EDS data over a regular grid with 8 μm spacing. Automated search and identification of PGM was performed by the bright phase search method using an 1 μm step. The composition of platinum-group minerals was determined by Cameca SX–100 equipped with four wavelength-dispersive X-ray spectrometers (IG CAS) using the accelerating voltage of 15 kV, a beam current of 20 nA and focused beam diameter of 1 μm . The following elements were analysed (spectrum lines, standards, spectrometer crystals, and counting time are given in the parentheses): Pd (L_{α} , LPET, 40 s), Pt (M_{β} , LPET, 90 s), Te (L_{α} , LPET, 10 s), Bi (M_{α} , LPET, 10 s), S (K_{α} , markasite, LPET, 10 s), Fe (K_{α} , Fe_2O_3 , LLIF, 10 s), Co (K_{α} , LLIF, 10 s), Ni (K_{α} , LLIF, 10 s), Cu (K_{α} , LLIF, 20 s), Se (L_{α} , TAP, 10 s), As (L_{β} , GaAs, TAP, 10 s), Sb (L_{α} , LPET, 10 s). The X-phi (Merlet 1994) correction procedure was used for spectra processing.

3.3. Highly siderophile element and Re–Os isotopic analysis

Approximately 1–2 g of whole-rock sample powder (dolerite) and 15–30 mg (ore) was sealed with appropriate amounts of ^{185}Re – ^{190}Os and ^{191}Ir – ^{99}Ru – ^{105}Pd – ^{194}Pt spikes and digested in pre-cleaned Carius Tube using 4 ml concentrated HCl and 5 ml concentrated HNO_3 at 260 °C (sulphides at 230 °C) for ~72 hours (Shirey and Walker 1995). After decomposition, osmium was extracted from

aqua regia solution into CHCl_3 , back-extracted into 4 ml of concentrated HBr and dried (Cohen and Waters 1996). The Os fraction was purified by microdistillation, using CrO_3 and HBr (Birck et al. 1997).

In order to ensure full extraction of rhenium and Ir, Ru, Pd and Pt from the dolerite sample, remaining undecomposed silica-rich residue was treated by desilicification procedure using HF–HCl mixture following Dale et al. (2008) and Ishikawa et al. (2014). Then, the Ir, Ru, Pd, Pt and Re from desilicified and sulphide-fractions were separated by anion exchange chromatography using AG 1×8 resin (BioRad).

Osmium concentrations and $^{187}\text{Os}/^{188}\text{Os}$ ratios were obtained by N-TIMS technique (Creaser et al. 1991; Völkening et al. 1991) using Finnigan MAT 262 mass spectrometer housed at the Czech Geological Survey (CGS). In run precision for $^{187}\text{Os}/^{188}\text{Os}$ ratios was always better than ± 0.2 % (2 SE). The measured Os isotopic ratios were corrected offline for mass fractionation using $^{192}\text{Os}/^{188}\text{Os} = 3.08271$ (Shirey and Walker 1998) and spike/blank contributions. External reproducibility was monitored by analyses of UMCP Os solution yielding $^{187}\text{Os}/^{188}\text{Os}$ of 0.113827 ± 21 ($n = 23$) and 0.113718 ± 51 ($n = 16$) for Faraday cups and electron multiplier measurements, respectively.

Iridium, Ru, Pt, Pd and Re concentrations were determined using sector field ICP–MS (Element 2, Thermo Scientific, Germany) at the IG CAS. The internal precision was always better than 0.3%. Isotopic fractionation was corrected for by linear law and measurements of natural Ir, Ru, Pt and Re standard solutions. The total procedural blanks were 0.1 pg for Os, 3 pg for Ir, 2 pg for Ru, 11 pg for Pt, 9 pg for Pd and 2 pg for Re. Accuracy of the method was checked by the analyses of TDB-1 diabase reference material (CANMET, Canada) yielding values similar to that presented by Ishikawa et al. (2014).

3.4. Sulphur isotopic analysis

Sulphides were oxidized by CuO to SO_2 at 800 °C according to the procedure described by Grinenko (1962), and released SO_2 was then measured on a Finnigan MAT 251 mass spectrometer at the CGS. The S isotope ratios are reported in the standard δ notation (in per mil), expressed relative to the CDT and V-PDB standards. Precision and accuracy of the $\delta^{34}\text{S}$ data is $\pm 0.2\%$ as determined by repeated analyses of the CDT international standard.

3.5. U–Pb zircon geochronology

Approximately 35 kg sample of the dolerite ROZ1 was used for the zircon separation. Zircon grains were extracted using conventional mineral separation techniques (jaw crushing, Wilfley concentration table, and finally,

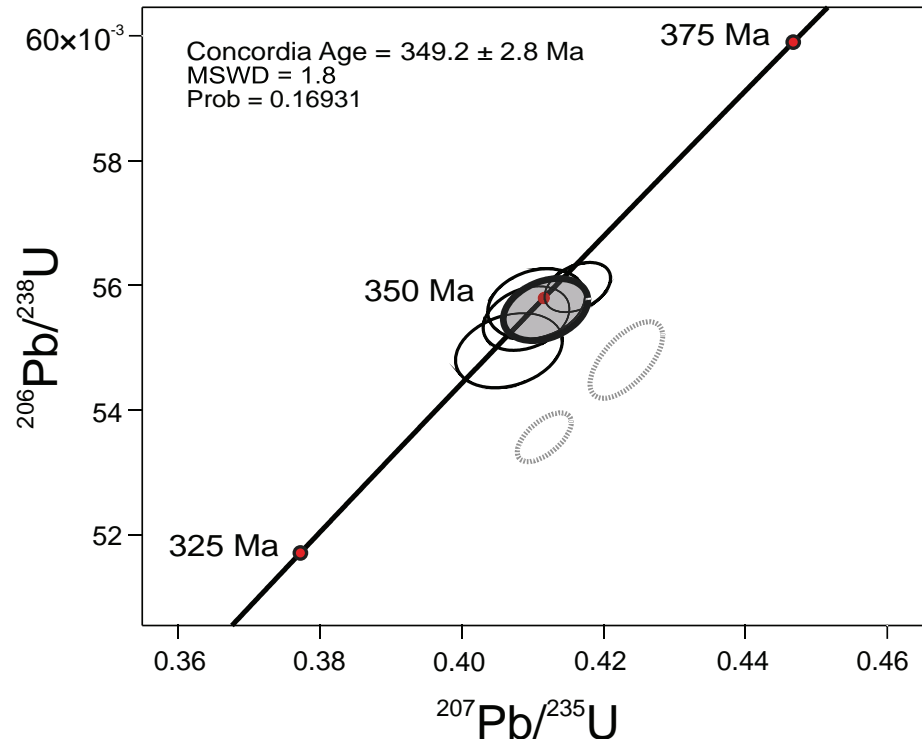


Fig. 2 U–Pb concordia diagram and calculated concordia ages for magmatic zircons (LA-ICP-MS data) from ROZ1 dolerite. All data are plotted with 2σ uncertainties. Two discordant ellipses (dashed) were excluded from the U–Pb age calculation.

magnetic and heavy liquid separations). Handpicked zircon grains were mounted in one-inch epoxy-filled blocks and polished. Internal zircon structure, zoning patterns and possible presence of older inherited components in individual grains was checked by cathodoluminescence (CL) imaging using scanning electron microscope Tescan Mira 3GMU at the CGS.

An Element 2 high-resolution sector field mass spectrometer (Thermo Scientific) coupled with a 213-nm NdYAG UP-213 laser ablation system (New Wave Research) at the IG CAS was used to acquire the Pb/U isotopic ratios. Samples were ablated in an in-house small-volume ablation cell, construction inspired by a conception of Kooijman et al. (2012). The laser was fired at a repetition rate of 5 Hz, using a spot size of 30 μm and a fluence of $\sim 4\text{--}5 \text{ J/cm}^2$. Acquisitions for all measured samples consisted of a 35 s measurement of blank followed by U and Pb signals from zircons for another 40 s. Data were collected for masses 204, 206, 207, 208, 232 and 238 using both analogue and ion counting modes of the SEM detector, one point per mass peak and relevant dwell times per mass of 10, 15, 30, 10, 10 and 15 ms. The sample introduction system was modified using Y-piece tube attached to the back end of the plasma torch and connected to the helium gas line carrying the sample from the laser cell. The Hg impurities in the carrier He gas, which can cause isobaric interference of ^{204}Hg on ^{204}Pb , were reduced by using in-house made gold-coated sand trap. The relative contribution of common Pb to total Pb was less than 0.1 % and, therefore, no common Pb cor-

rection was applied to the data. Elemental fractionation and instrumental mass bias were corrected by normalization of internal U–Pb calibration zircon standard 91500 (1065 Ma; Wiedenbeck et al. 1995) and reference natural zircon standard GJ-1 (609 Ma; Jackson et al. 2004, 603 Ma; Kylander-Clark et al. 2013) periodically analysed during the measurement. The obtained concordia ages of these standards $1065 \pm 2 \text{ Ma}$ (2σ) and $607 \pm 1 \text{ Ma}$ (2σ) correspond well within the errors to published zircon standards ages. Raw data reduction and age calculations, including corrections for baseline, instrumental drift, mass bias and down-hole fractionation, were carried out using the computer program Iolite (v. 3.0; Paton et al. 2011). The U–Th–Pb isotopic data and zircon ages shown in conventional concordia diagram (Fig. 2) were also generated by the same software with VisualAge add-in (Petrus and Kamber 2012). For the data presented here, blank intensities and instrumental bias were interpolated using an automatic spline function while down-hole inter-element fractionation was corrected using an exponential function.

4. Results

4.1. Petrography and trace-element composition of dolerites

The Rožany dolerite shows sub-ophitic texture dominantly consisting of amphibole and plagioclase mak-

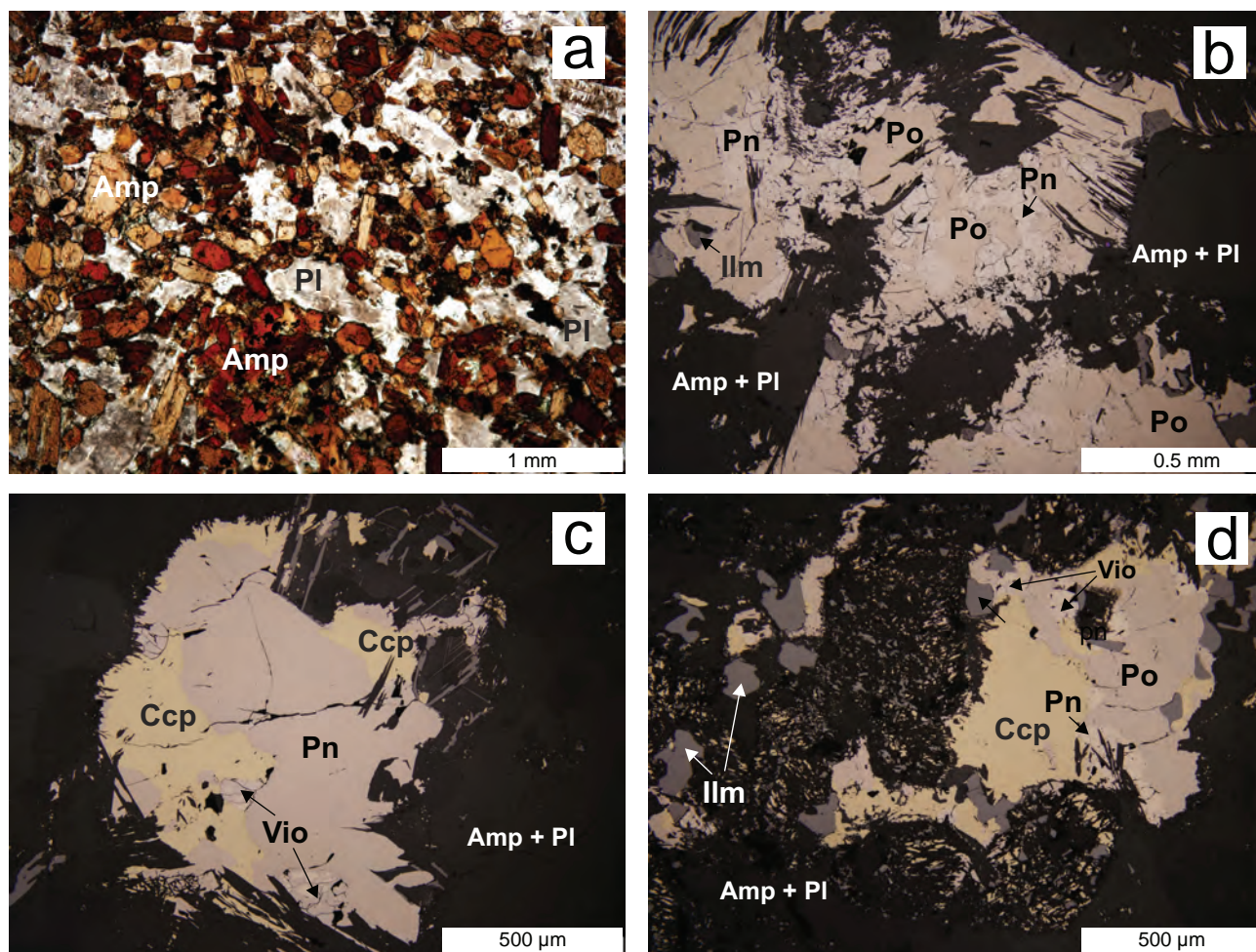


Fig. 3 Photomicrographs of the studied samples. **a** – Texture of barren dolerite in plain polarized light. **b** – Typical texture of massive Ni–Cu ore from Rožany. Note partial dissolution of pyrrhotite and pentlandite along some of the grain edges. **c** – Detail of chalcopyrite–pentlandite grain with violarite replacing pentlandite. **d** – Complex ore assemblage consisting of all ore-bearing minerals: pyrrhotite, pentlandite, chalcopyrite and violarite. Amp – amphibole, Pl – Plagioclase, Po – pyrrhotite, Pn – pentlandite, Ccp – chalcopyrite, Vio – violarite, Ilm – ilmenite.

ing up to 90 vol. % of the total minerals (Fig. 3a). Additionally, subordinate amounts of clinopyroxene and biotite (<5 vol. %) are present. Brown amphibole typically forms tabular and/or anhedral grains up to 1 mm in length. Plagioclase is strongly replaced by sericite and chlorite. Opaque minerals are represented by abundant ilmenite and magnetite accompanied by pyrrhotite. Needle-like apatite forms common accumulations associated with plagioclase. Among other accessory minerals, zircon, baddeleyite, thorite and titanite were identified.

Trace-element abundances in the barren dolerites are given in Tab. 1 whereas rare-earth element (REE) and multielement trace-element patterns, both normalized to Primitive mantle (McDonough and Sun 1995), are shown in Fig. 4. Studied dolerites exhibit light rare element (LREE)-enriched patterns with high La_N/Yb_N ratios of ~ 16.7 and no Eu anomaly. Extended trace-element patterns show enrichment in all incompatible elements

with respect to primitive mantle, notably Rb, Nb, U, Th and Sr but markedly negative Pb anomaly (Fig. 4). No fractionation was observed between Zr and Hf.

4.2. Zircon U–Pb geochronology

Unfortunately, only a limited number of zircons was successfully extracted from the sample ROZ1 and dated using laser-ablation ICP-MS U–Pb analysis (Tab. 2, Fig. 2). Most of the studied grains are typical morphological zircon populations: clear prismatic (euhedral to needle-like, Fig. 5a), pale brown prismatic–stubby (Fig. 5b) or equant–oval (Fig. 5d) grains. Cathodoluminescence images (CL) show several types of magmatic zoning. Partially preserved complex oscillatory growth zoned zircons are penetrated by zones of recrystallization (Fig. 5e), while some larger stubby grains consist of oscillatory-zoned zircon surrounding unzoned xenocrystic cores (Fig. 5a).

Tab. 1 Trace-element and Re–Os isotopic data for barren dolerites from Rožany

Sample	ROZ	ROZ 1/1
Li (ppm)	21	21
Sc	12.2	10.3
V	266	228
Cr	136	100
Co	54	45
Ni	194	129
Rb	24	20
Sr	859	927
Y	22	24
Zr	251	267
Nb	51	58
Cs	1.4	0.94
Ba	331	339
La	33	36
Ce	72	78
Pr	9.4	10
Nd	41	45
Sm	9.1	9.7
Eu	3.0	3.2
Gd	9.0	9.8
Tb	1.3	1.4
Dy	5.7	6.0
Ho	0.89	0.95
Er	2.3	2.4
Tm	0.23	0.25
Yb	1.4	1.5
Lu	0.18	0.19
Hf	6.6	6.9
Ta	3.1	3.5
Pb	3.0	3.0
Th	2.9	3.0
U	0.63	0.67
Os (ppb)	0.094	–
Ir	0.10	–
Ru	0.20	–
Pt	1.26	–
Pd	0.91	–
Re	0.62	–
¹⁸⁷ Re/ ¹⁸⁸ Os	32.7	–
¹⁸⁷ Os/ ¹⁸⁸ Os	0.3223	–
γ Os (349 Ma)	+5.6	–

U–Pb zircon dating of sample ROZ1 yielded concordant ages between *c.* 338 Ma and 352 Ma (Tab. 2) and weighted mean concordia age of 349 ± 3 Ma (2σ ; four analyses; Fig. 2) that is interpreted as timing the intrusion. Excluded from this calculation were two zircon analyses (dashed ellipses on Fig. 2) that are discordant. The lead loss, possibly associated with considerable fluid movement subsequent to magmatic crystallization, is the most likely explanation of their discordant composition. We have also detected two inherited zircon cores, which are not visualized on concordia diagram, that yielded concordant ages of *c.* 600 and 650 Ma, respectively. The studied grains have Th/U ratios (Tab. 2) of 0.3–1.4 (average 0.6) similar to magmatic zircons that are usually characterized by Th/U > 0.5 (Hoskin and Schaltegger 2003 and references therein).

4.3. Sulphide petrography, modal compositions and platinum-group minerals

The Ni–Cu ore is composed of large (3–5 mm), irregular and brecciated pyrrhotite flakes enclosing silicates and anhedral grains of magnetite–ilmenite with high degree of fragmentation and disorientation (Fig. 3b). Resorption is very common along the silicate–pyrrhotite boundaries. Pentlandite forms small (< 0.3 mm) rounded grains enclosed in pyrrhotite, which are commonly replaced by violarite (Fig. 3c). Violarite also forms thin vein-lets penetrating large pyrrhotite flakes. Chalcopyrite is rare, but if present, it is concentrated on the rims of large pyrrhotite flakes and/or forms individual small, highly resorbed patches (< 0.3 mm) within silicates. No exsolution lamellae and/or flames were observed in any of the studied sulphide phases. The Cu–Ni ore shows similar texture but differs by the predominance of chalcopyrite over pentlandite. The latter mineral is commonly replaced by violarite forming brecciated texture. Chalcopyrite typically forms millimetre-sized irregular fillings and equant grains within large pyrrhotite grains (Fig. 3d) or pyrrhotite–chalcopyrite intergrowths less than 1 mm across. In some pyrrhotite grains, very thin (< 10 μ m) exsolution lamellae of pentlandite were

Tab. 2 Laser-ablation ICP-MS U–Pb data for zircons from the Rožany dolerite (sample ROZ1)

Anal. No.	Corrected isotope ratios					Apparent ages (Ma)				U, Th and Pb content (ppm)						
	²⁰⁷ Pb/ ²³⁵ U	$\pm 1\sigma$	²⁰⁶ Pb/ ²³⁸ U	$\pm 1\sigma$	error corr.	²⁰⁷ Pb/ ²³⁵ U $\pm 1\sigma$	²⁰⁶ Pb/ ²³⁸ U $\pm 1\sigma$	Approx U $\pm 1\sigma$	Approx Th $\pm 1\sigma$	Approx Pb $\pm 1\sigma$	Th/U					
Sample ROZ1 (diorite)																
1	0.4060	0.0075	0.0538	0.0006	0.2810	346	6	338	4	272	4	128	4	22	1	0.5
2	0.4156	0.0046	0.0546	0.0004	0.3742	352	3	343	2	590	12	204	7.7	31	1.0	0.3
3	0.4098	0.0068	0.0545	0.0006	0.2090	348	5	342	3	563	11	143	6.7	22	1.0	0.3
4	0.4079	0.0061	0.0543	0.0005	0.29471	347	4	341	3	449	12	647	20	103	2.3	1.4
5	0.4124	0.0049	0.05348	0.00071	0.56686	351	4	336	4	1831	19	163	1	26	1	0.1
6	0.4229	0.0053	0.05437	0.00073	0.57881	358	4	341	5	1487	16	220.6	8	35	1.5	0.1

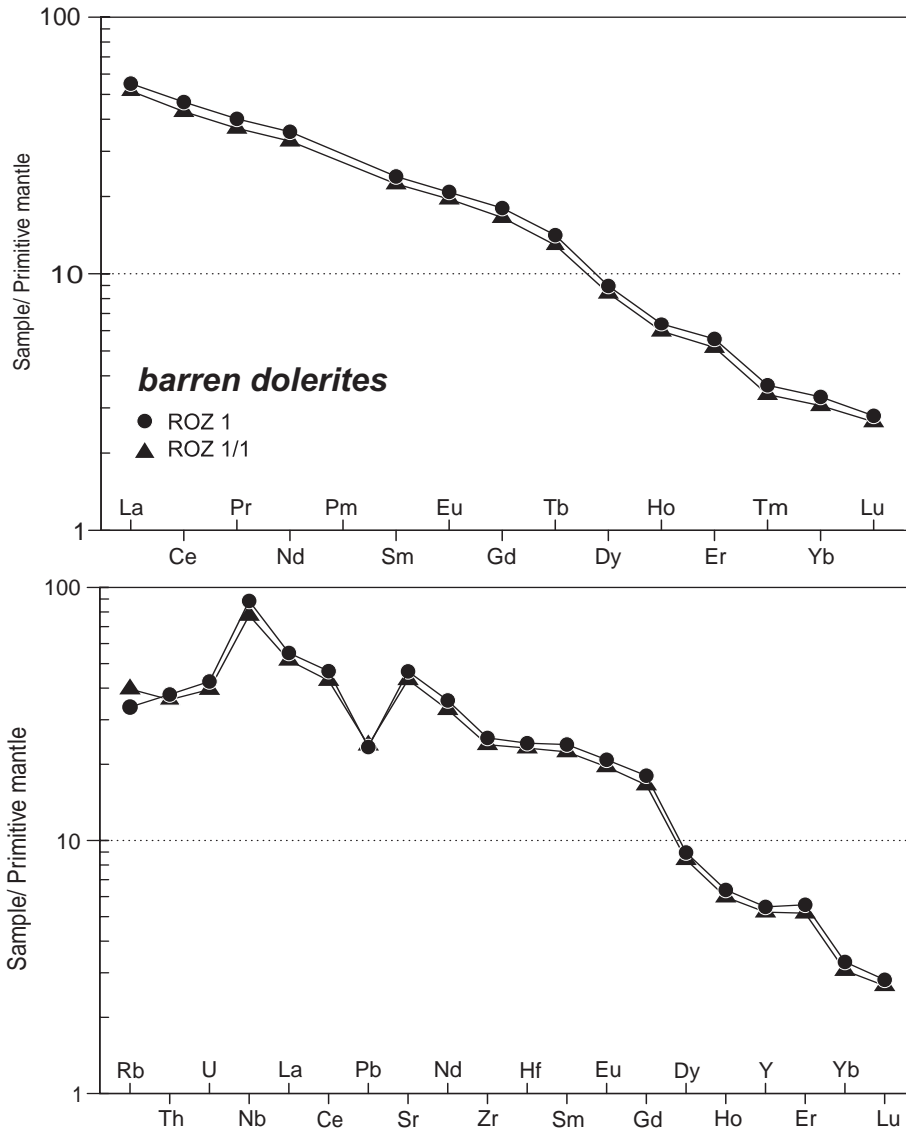
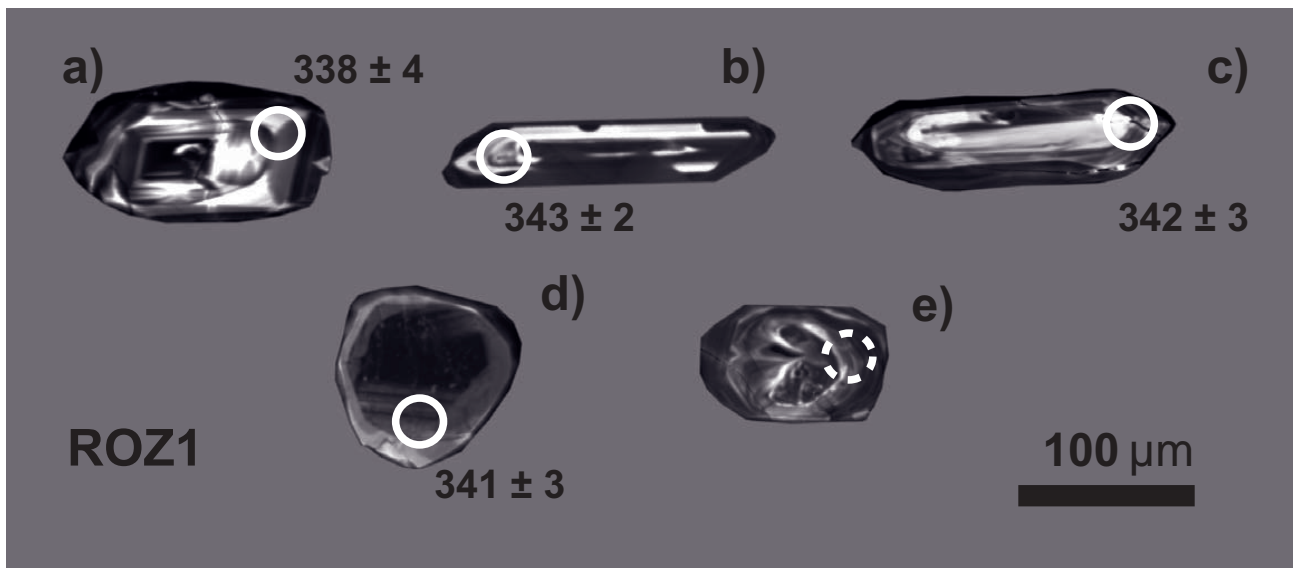


Fig. 4 Trace-element compositions of barren dolerites (normalized to Primitive mantle values of McDonough and Sun 1995).



Tab. 3 Sulphide modal compositions (vol. %, recalculated to 100 % sulphide fraction)

Sample	ROZ 2/1	ROZ 2/2	ROZ2/3	ROZ 3/1	ROZ3/2	ROZ 4/2	ROZ 4/1	ROZ 4/3
Ore type	massive Ni–Cu	massive Ni–Cu	massive Ni–Cu	massive Cu–Ni	massive Cu–Ni	massive Cu–Ni	disseminated Ni–Cu	disseminated Ni–Cu
Chalcopyrite	0.8	1.0	28	18	58	28	32	26
Pyrrhotite	84	81	59	70	35	61	52	62
Fe–Ni-sulphides	15	18	13	12	7	10	16	12
Total	100	100	100	100	100	100	100	100

Tab. 4 Compositions of platinum-group minerals detected in the Rožany ores (wt. %)

Sample	Rock	Mineral	Pd	Pt	Te	Bi	S	Fe	Ni	As	Sb	Total
ROZ 2/2	massive Ni–Cu ore	sperrylite	b.d.l.	53.95	0.72	b.d.l.	0.80	2.25	2.31	38.53	b.d.l.	98.57
ROZ 2/3	massive Ni–Cu ore	unknown Pt–As–Te phase?	b.d.l.	51.48	12.29	0.69	0.264	2.56	0.17	31.60	0.26	99.32
ROZ 2/3	massive Ni–Cu ore	moncheite	5.96	21.69	60.82	6.31	0.02	1.24	4.64	b.d.l.	0.10	100.76
ROZ 2/2	massive Ni–Cu ore	michenerite	24.10	b.d.l.	31.43	41.17	b.d.l.	2.14	b.d.l.	b.d.l.	0.13	96.84
ROZ 2/2	massive Ni–Cu ore	michenerite	23.56	b.d.l.	30.65	42.90	0.037	2.06	0.27	b.d.l.	0.23	97.64
ROZ 4/2	massive Cu–Ni ore	(Sb-rich) michenerite	24.44	b.d.l.	34.42	24.89	0.36	1.46	2.21	b.d.l.	12.17	99.94

b.d.l. = below detection limit

observed. The disseminated ores are characterized by predominance of pyrrhotite with variable amounts of chalcopyrite and pentlandite; subordinate violarite replaces pentlandite. The size of the sulphide grains, flakes and patches dispersed in the silicate matrix is typically less than 1 mm.

Sulphide modal compositions of the studied samples of Ni–Cu ores from the Rožany deposit are variable (Tab. 3). The highest amounts of Fe–Ni sulphides (15–18 vol. %) show massive Ni–Cu ores. Poorer are the disseminated ores, which contain 10–11 vol. % Fe–Ni sulphides. The massive Cu–Ni ores have 7–12 vol. % of Fe–Ni sulphides, but the highest amounts of pyrrhotite are typical of massive Ni–Cu ores (59–84 vol. %). The lowest contents of pyrrhotite are characteristic of massive Cu–Ni ores (35–70 vol. %), and disseminated ores have 52–62 vol. % of pyrrhotite. The chalcopyrite amounts are highly variable (18–58 vol. %) being lower in disseminated pyrrhotite–chalcopyrite ores (26–32 vol. %) and the lowest in massive Ni–Cu ores (0.8–28 vol. %).

Previous studies of Pašava et al. (2001) and Vavřín and Frýda (1998) identified several platinum-group minerals (PGM) such as sperrylite [PtAs₂] and unnamed Pd–Ni bearing tellurides [Pd₂(Ni,Fe)₂BiTe₆ and PdNi(Sb,Bi)Te₂] as principal carriers of the PGE mineralization. The PGM phases were usually detected in sulphides (predominantly in pyrrhotite and/or in chalcopyrite) and at the sulphide–silicates grain boundaries. Our detailed SEM study confirms common presence of sperrylite (Fig. 6a). Moreover, it also revealed moncheite [(Pt,Pd)

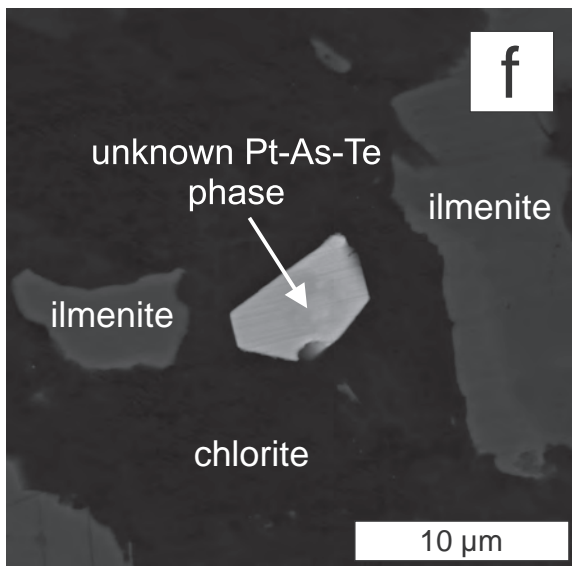
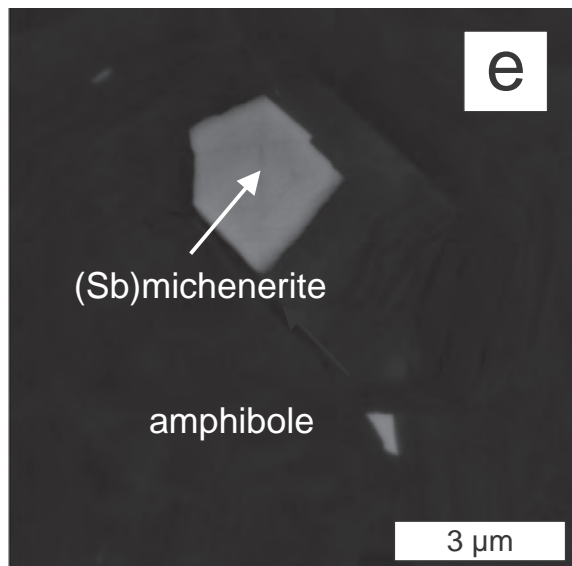
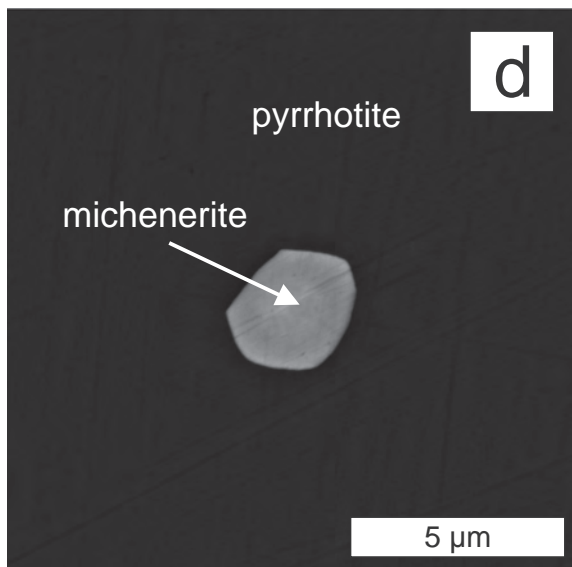
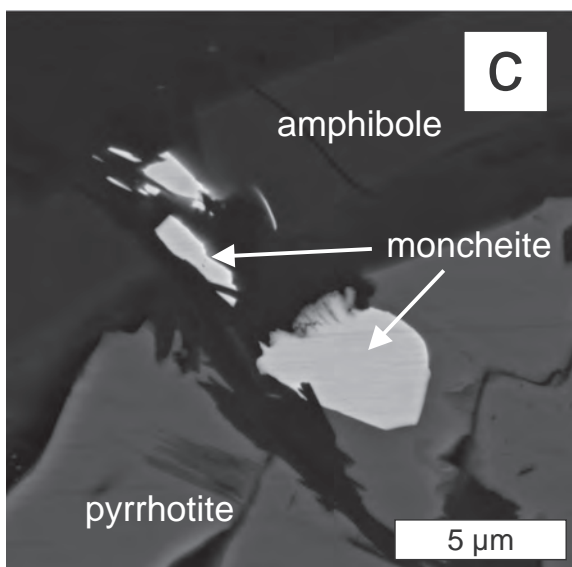
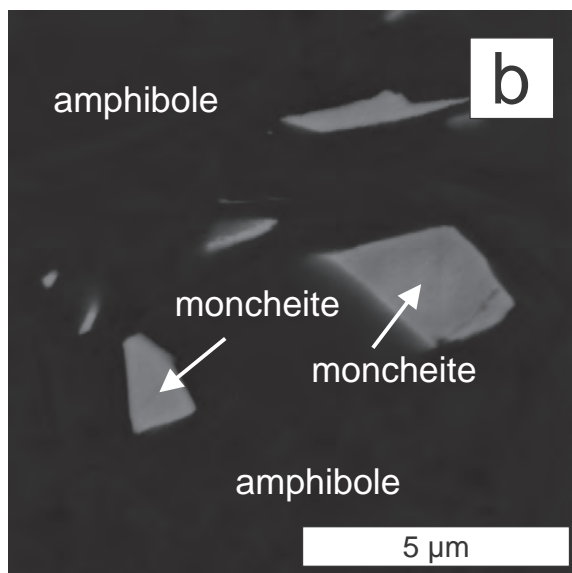
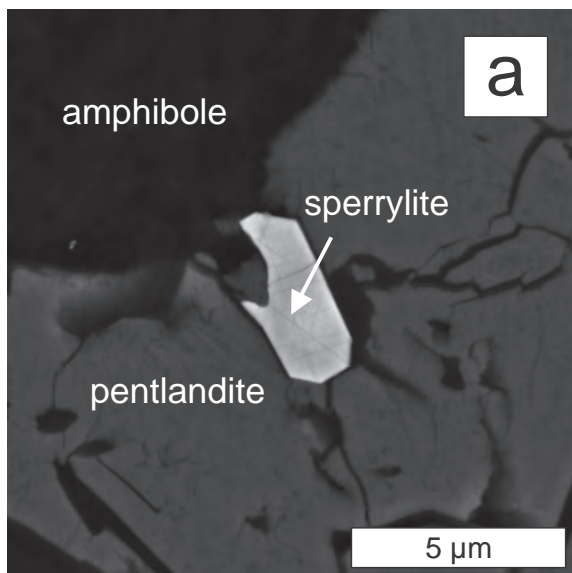
(TeBi)₂] grains (Fig. 6b–c) with elevated Fe and Ni contents (Tab. 4), and michenerite [(Pd)BiTe; Fig. 6d–e] with sometimes high Sb contents (e.g., up to 12.2 wt. %; Tab. 4) as common Pd- and Pt-bearing phases. Additionally, possible yet unknown Pt–As–Te phase (Fig. 6f) was identified; however, its composition (Tab. 4) may also be explained as a mixture of sperrylite and some Pt–Te phase (e.g., moncheite) which cannot be resolved due to its very small size. Automated SEM detection revealed that these PGM are located not only within all base-metal sulphides, but also in matrix silicates (e.g., Fig. 6b, e–f).

4.4. Trace elements in Rožany ores

Studied samples show variable concentrations of trace elements (Tab. 5). The samples of massive ores contain higher concentrations of Ni (1.0–1.9 wt. % and 0.3–0.8 wt. % for Ni–Cu and Cu–Ni ores, respectively) than the disseminated ores (0.8–0.9 wt. %). Similarly, the Cr and Co concentrations are generally higher (525–831 ppm and 190–608 ppm, respectively) in massive than in disseminated ores (470–609 ppm and 31–341 ppm, respectively). The massive ores are also characterized by relatively variable concentrations of Cu ranging from very high in Cu–Ni types (1.5–2.1 wt. %), through intermediate in disseminated ores (0.5–0.7 wt. %) to the lowest in massive Ni–Cu ores (0.2–0.8 wt. %). Bismuth and Te also show variable distribution with the most variable concentrations found in massive Ni–Cu ores (0.80–5.45 ppm for Bi and 0.91–4.98 ppm for Te), on average slightly higher values found in disseminated ores (1.55–2.34 ppm and 1.48–2.34 ppm for Bi and Te, respectively) than homogeneous contents found in Cu–Ni ores (2.46–3.15 ppm for Bi and 2.04–2.56 ppm for Te). Arsenic concentrations varied among all studied ore samples between 0.49 and 1.61 ppm. The lowest

⇐

Fig. 5 Representative cathodoluminescence images of the dated zircon grains from the studied sample (ROZ1). Laser-ablation ICP-MS analysis spots are marked with concordant ²⁰⁶Pb/²³⁸U ages with 1σ uncertainties. Dotted in grain e) is the analytical spot that was not included in the concordia age calculation (see text for explanation).



Tab. 5 Trace-element and highly siderophile element concentrations along with Re–Os isotopic data of ores from Rožany

Sample	ROZ 2/1	ROZ 2/2	ROZ2/3	ROZ 3/1	ROZ 3/2	ROZ 4/2	ROZ 4/1	ROZ 4/3
Ore type	massive Ni–Cu	massive Ni–Cu	massive Ni–Cu	massive Cu–Ni	massive Cu–Ni	massive Cu–Ni	disseminated Ni–Cu	disseminated Ni–Cu
Ni (wt. %)	1.92	1.65	0.99	0.84	0.31	0.69	0.87	0.83
Cu	0.56	0.21	0.79	1.51	2.13	1.46	0.72	0.48
Sb (ppm)	0.17	0.10	0.48	0.52	0.56	0.60	0.34	0.81
Te	0.91	1.10	4.98	2.14	2.04	2.56	2.34	1.48
Bi	0.80	1.20	5.45	2.46	2.51	3.15	2.34	1.55
As	0.58	0.85	1.61	0.59	0.49	0.59	1.16	0.88
Se	17.9	15.4	16.3	13.3	9.91	12.8	11.7	9.73
V	202	194	220	228	227	226	228	121
Cr	525	831	674	763	661	639	470	609
Co	506	608	352	373	190	322	321	341
Zn	114	108	187	253	155	151	135	159
Pb	17.5	24.5	82	66	75	78	44	26.2
Os (ppb)	22.8	25.6	–	4.95	2.89	4.26	16.5	–
Ir	11.4	13.3	–	2.6	1.58	2.33	8.48	–
Ru	28.8	31.2	–	4.9	2.94	4.49	18.4	–
Pt	15.9	39.0	–	67.9	40.3	85.1	98.5	–
Pd	67.2	65.2	–	109.5	99.7	104.7	29.3	–
Re	57.5	61.4	–	12.3	6.1	10.0	12.1	–
¹⁸⁷ Re/ ¹⁸⁸ Os	12.5	11.9	–	12.2	10.3	11.6	3.56	–
¹⁸⁷ Os/ ¹⁸⁸ Os	0.365	0.357	–	0.292	0.271	0.268	0.207	–
γOs (349 Ma)	+134	+131	–	+77	+69	+61	+50	–

concentrations of some compatible elements (e.g. Cr and Ni) exhibit barren dolerites.

4.5. Platinum-group elements and rhenium concentrations

Generally, the highest contrast in platinum-group element (PGE) and rhenium contents is between two types of massive ores (Tab. 5). Primitive-mantle normalized (McDonough and Sun 1995) patterns for Ni, Cu, Re and PGE of the Rožany ores are shown in Fig. 7. The Ni–Cu ores contain very high levels of I-PGE (Os: 22.8–25.6 ppb, Ir: 11.4–13.3 ppb, Ru: 28.8–31.2 ppb) and Re (57.5–61.4 ppb), much lower Pt contents (15.9–39.0 ppb) and only slightly elevated Pd concentrations (65.2–67.2 ppb). This fact illustrates low Pd/Ir ratios (4.9–5.9). On the contrary, Cu–Ni ores are characterized by high Pt and Pd concentrations (67.9–85.1 ppb and 99.7–109.5 ppb, respectively), but much lower contents of I-PGE. All these features result in relatively high Pd/Ir ratios of 42–63. The lowest PGE contents were detected in the barren dolerite (0.094–1.26 ppb, Tab. 1). Rhenium

concentrations are variable with the highest identified in massive Ni–Cu ores (57.5–61.4 ppb) and much lower in massive Cu–Ni and disseminated ores (6.1–12.3 ppb). The lowest Re concentration was found in the barren dolerite (0.62 ppb).

4.6. Osmium and sulphur isotopic compositions

The obtained ¹⁸⁷Os/¹⁸⁸Os ratios vary broadly in the range of 0.2073 and 0.3645 (Tab. 5) with the highest values found in massive Ni–Cu ores (0.357–0.367) and barren dolerite (0.322, Tab. 2). The lowest ¹⁸⁷Os/¹⁸⁸Os ratios are characteristic of disseminated ores (0.207–0.268). In comparison, the ¹⁸⁷Re/¹⁸⁸Os ratios of massive Ni–Cu ores are very homogeneous (11.9–12.5), whereas the disseminated ore and barren dolerite yield much lower (3.56) and higher (32.6) ones, respectively. The γOs values at 349 Ma (calculated using chondritic composition of Shirey and Walker 1998) range from +5.6 for barren dolerite to highly radiogenic values in ores (from +50 to +134) with the highest values found in massive Ni–Cu ores.

Sulphur isotope data for pyrrhotite and chalcopyrite from massive Cu–Ni ores are given in Tab. 6. Overall, all analysed sulphides yield rather homogeneous δ³⁴S values in the range of –2.7 and +0.1 ‰ with no resolvable difference between different types of ore and/or sulphide mineral.

↩

Fig. 6 Detected platinum-group minerals from the Rožany Ni–Cu–(PGE) mineralization. **a** – Sperrylite (PtAs₂) enclosed in pentlandite. **b** – Moncheite grains [(Pt,Pd)(TeBi)₂] in amphibole. **c** – Partially resorbed moncheite on the border between chalcopyrite and pyrrhotite. **d** – Michenerite (PdBiTe) enclosed in pyrrhotite. **e** – Sb-michenerite grains enclosed in amphibole. **f** – Possible unknown Pt–As–Te phase in chlorite.

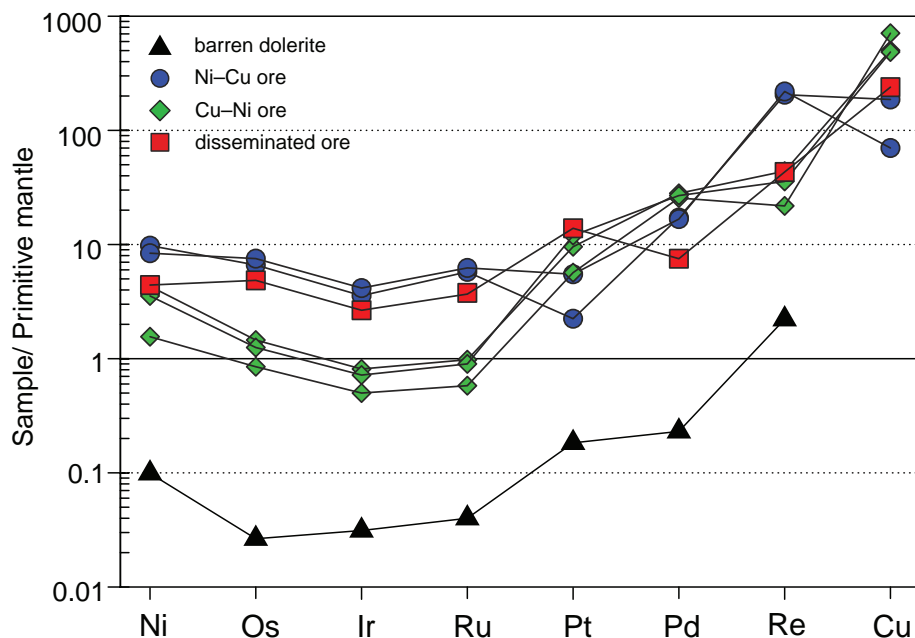


Fig. 7 Highly siderophile and chalcophile element compositions of the studied rocks (normalized to Primitive mantle of McDonough and Sun 1995).

5. Discussion

5.1. Constrains on the age and magma sources of the barren dolerite

The age of gabbroic dykes in the Lusatian Granitoid Complex has been poorly constrained by whole-rock K–Ar and single zircon evaporation Pb–Pb methods at ~390–400 Ma (Kramer 1977; Kindermann et al. 2003). On the other hand, the Lusatian lamprophyric dykes gave Ar–Ar ages on amphibole of 325.5 ± 2.9 Ma and 336.7 ± 3.9 Ma (Abdelfadil et al. 2013).

In contrast, our new *in-situ* U–Pb zircon data for the Rožany dolerite yield the age of 349 ± 3 Ma which is much lower than previous K–Ar/Pb–Pb data. The reason for the discrepancy between the existing Pb–Pb and our new U–Pb zircon data can be associated with the detected inherited zircon cores (~600 and 650 Ma) and/or zircon modification by hydrothermal alteration, effects of which are visible in the CL images. Therefore, our *in-situ* data should be considered more reliable and obtained age suggests rather closer temporal relationship of dolerite dykes to lamprophyres in the Lusatia.

Tab. 6 Sulphur isotopic compositions of sulphides from Rožany

Sample	Ore type	Mineral	$\delta^{34}\text{S}$ (‰)
ROZ 2/1	massive Ni–Cu	pyrrhotite	–2.6
ROZ 2/2	massive Ni–Cu	pyrrhotite	–1.2
		chalcopyrite	–1.5
ROZ 3/1	massive Cu–Ni	chalcopyrite	–2.7
ROZ 3/2	massive Cu–Ni	chalcopyrite	+0.1
		pyrrhotite	–2.0
ROZ 4/2	massive Cu–Ni	pyrrhotite	–2.3

Chemical composition of barren dolerites can provide important insights into the composition of parental basaltic magma sources. When compared to the Primitive mantle, the Rožany dolerites are characterized by high degree of LREE enrichment ($\text{La}_N/\text{Yb}_N \sim 16.7$) and absence of Eu anomaly. In combination with the observed enrichment in other incompatible trace elements (e.g., Rb, Sr; Fig. 4), this suggests derivation of the parental magmas from enriched (metasomatized) mantle source.

Mafic dykes of gabbroic composition presumably derived from subduction-related metasomatized mantle are common in Lusatia. Even though they are accompanied by calc-alkaline lamprophyres (Abdelfadil et al. 2013), they show rather tholeiitic compositions with much lower levels of incompatible elements (e.g., LREE–MREE, Ba, Sr, Nb) than the Rožany dolerites. In comparison, composition and mineralogy (e.g., predominant amphibole, accessory apatite) of studied dolerites from Rožany are rather similar to the calc-alkaline lamprophyric dykes (Abdelfadil et al. 2013) suggesting different mantle source and/or degree of crustal contamination when compared to other gabbroic dykes in the area. More extensive dataset for barren dolerites would be needed for a modelling of assimilation-fractional crystallization process. Nevertheless, as Re–Os isotopic compositions of mantle-derived magmas are very sensitive to crustal contamination (e.g., Shirey and Walker 1998), they have a potential to distinguish between enriched mantle source and high-level of melt contamination which should result in highly radiogenic γOs . Using zircon U–Pb age of 349 Ma leads to initial γOs value of +5.6 which is very similar to the present-day Enriched Mantle reservoir 2 with γOs of +7.1 (Shirey and Walker 1998). This may imply

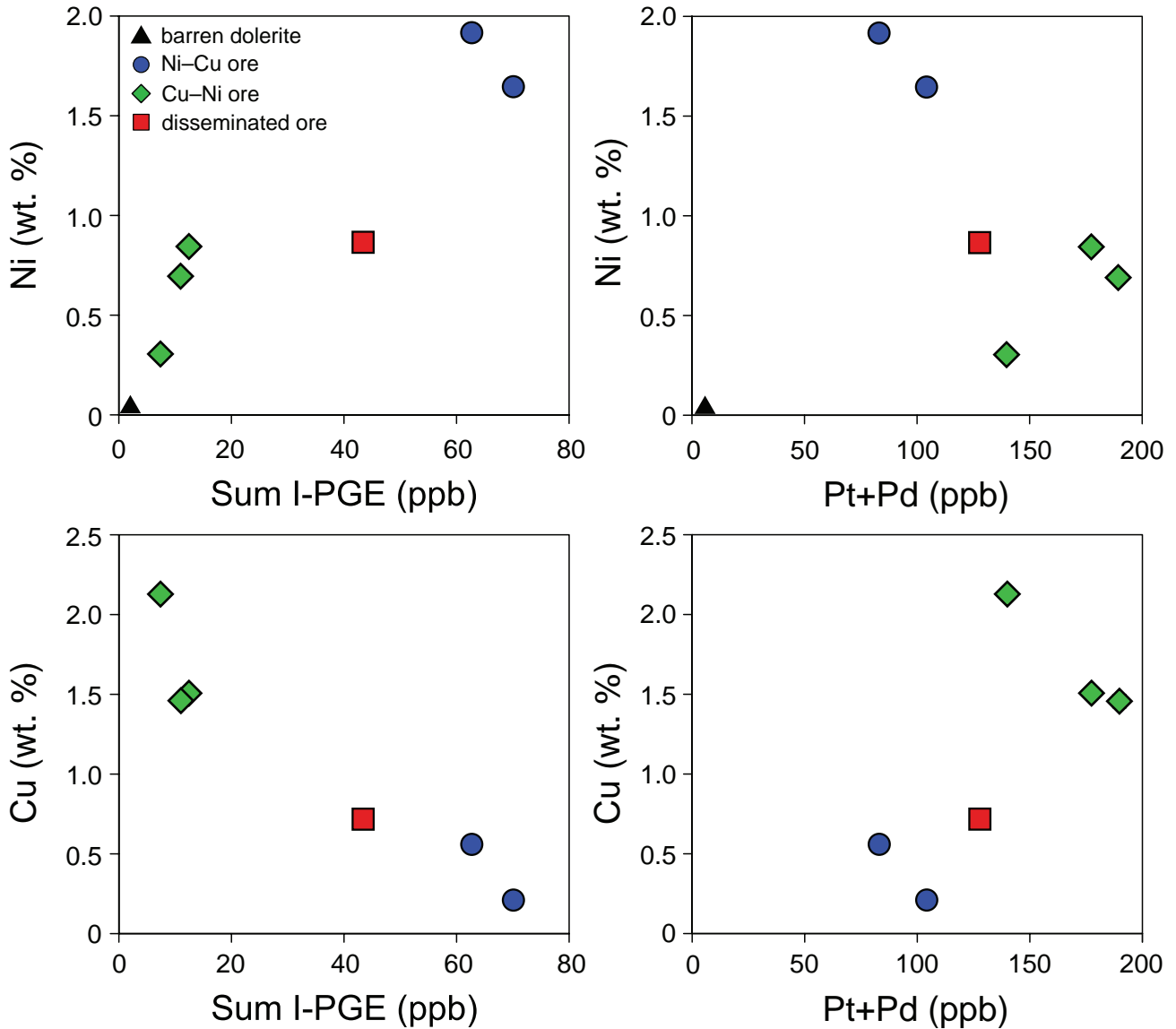


Fig. 8 Variations of I-PGE (Os, Ir, Ru) and Pt + Pd concentrations with Ni and Cu contents.

derivation of Rožany dolerites from subduction-related upper mantle, which is in agreement with conclusions of Abdelfadil et al. (2013).

5.2. The origin of PGE mineralization and Re–Os isotopic signatures

The Rožany–Kunratice mineralization represents a Ni–Cu–(PGE) magmatic/hydrothermal deposit associated with mafic rocks with mineralogy similar to other PGE deposits worldwide (e.g., Cawthorn et al. 2002; Farrow and Lightfoot 2002; Komarova et al. 2002 and references therein). Association of base-metal sulphides represented by pyrrhotite, pentlandite and chalcopyrite is typical of magmatic sulphides formed by the separation of sulphur-saturated melts at the

final stages of parental melt differentiation. In other words, it is very likely that crystallization of silicate minerals (including zircon) and sulphides was nearly contemporaneous.

Presence of violarite can be attributed to either supergene and/or hydrothermal alteration of pentlandite (Tenailleau et al. 2006) or this mineral may have formed as a primary exsolution phase from pentlandite (Grguric 2002). At Rožany–Kunratice, violarite clearly replaces pentlandite grains and/or forms secondary veinlets in large pyrrhotite grains. This suggests important role of hydrothermal activity, which was also most likely responsible for the origin of very common resorbed rims of all observed base-metal sulphides (e.g., Fig. 3b–c). As shown above, the PGM from Rožany are not only enclosed in all identified base-metal sulphides, but

they are also very common in silicate matrix minerals such as amphibole and/or chlorite. This indicates that also formation at least some of the PGM was closely associated with late-stage hydrothermal processes and they may be the products of the remobilization from the primary base-metal sulphides and/or their enclosed PGM. Further evidence for late-stage remobilization of sulphides is presence of thin pyrite-bearing veinlets cross-cutting main base-metal mineralization and impregnations of carbonate and quartz associated with hydrothermal alteration of primary silicate minerals (Pašava et al. 2001).

Association of individual PGE with different ore types is illustrated in Fig. 8. The I-PGE contents positively correlate with Ni values and abundances of Fe–Ni sulphides (not shown), but negatively with the Cu contents. The absence of I-PGE-bearing minerals within the PGE mineralization indicates that the I-PGE were most likely concentrated in Ni-bearing sulphides in the form of solid solution. For example, pentlandite can accommodate I-PGE at tens of ppm levels (e.g., Godel et al. 2007). In comparison, Ni-rich ores contain the lowest Pt–Pd contents whereas Cu–Ni ores tend to be richest in Pt and Pd. Except one sample, Pt–Pd contents broadly correlate with chalcopyrite modal abundance. When taking into account the common presence of Pt- and Pd-bearing minerals, it seems that Pt and Pd budgets are predominantly controlled by their own phases combined with a limited role of chalcopyrite.

The nature and source of PGE can be best examined via Re–Os isotopic compositions. The studied suite of massive and disseminated ores shows highly variable $^{187}\text{Os}/^{188}\text{Os}$ contrasting with mutually well comparable $^{187}\text{Re}/^{188}\text{Os}$ (except one value; Tab. 5). This results in highly variable γOs (349 Ma) values of +50 to +134. The magnitude and variability of these values clearly argue for a significant contribution of crustal material to parental melts as described also from other Ni–Cu–(PGE) deposits worldwide (e.g., Sudbury – Morgan et al. 2002; Pechenga – Walker et al. 1994). However, the observed $^{187}\text{Os}/^{188}\text{Os}$ compositions cannot come from a heterogeneous mantle source (very radiogenic γOs found in comparison to all mantle reservoirs) or reflect crustal contamination prior to the intrusion which would lead to uniform enrichment of ^{187}Os in the resulting melt (Walker et al. 1994). In addition, sulphur isotopic data for major sulphides (pentlandite, chalcopyrite, and pyrrhotite) show a narrow range of $\delta^{34}\text{S}$ from –2.7 to +0.1, which is similar to world-class sulphur-poor Ni–Cu–(PGE) deposits (e.g., Bushveld, Stillwater) and/or Sudbury (Ripley and Li 2003). These values argue for a homogenous source of mantle-derived magmatic sulphur without obvious mixing with external sources (e.g., granites and/or sediments). Crystallization of

mafic, sulphur-saturated melt in a closed system should lead to isochronous Re–Os relationship among samples within the studied suite. In turn, scattered variation between $^{187}\text{Re}/^{188}\text{Os}$ and $^{187}\text{Os}/^{188}\text{Os}$ for all rocks studied here (Fig. 9a) suggests either variable amounts of crustal material assimilated or modification of Re–Os systematics during post-emplacement hydrothermal alteration. If barren dolerite and surrounding Lusatian granitoids are considered to be representative of a parental melt and assimilant, respectively, their interaction should lead to development of a well-defined mixing trend in Os– γOs space as continental crust has typically very low Os content paralleled by very high γOs (e.g., Esser and Turekian 1993; Peucker-Ehrenbrink and Jahn 2001). In contrary, an opposite, rather scattered trend can be rec-

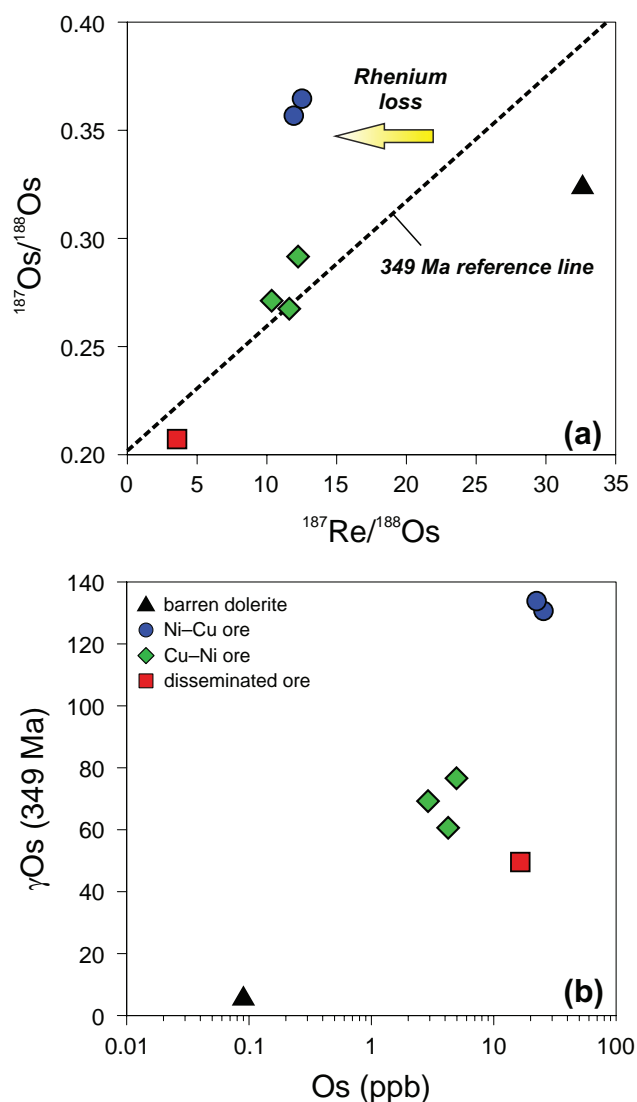


Fig. 9 Re–Os isotopic diagrams. **a** – $^{187}\text{Re}/^{188}\text{Os}$ vs. $^{187}\text{Os}/^{188}\text{Os}$ (isochron) diagram for the Rožany ores and barren dolerite. **b** – Variations of Os contents vs. initial γOs values calculated at 349 Ma.

ognized in Rožany with the highest Os contents found in the Ni-rich ores characterized by the highest γ Os values (Fig. 9b). Therefore, modification of Re–Os systematics during post-crystallization processes seems to be a more plausible explanation. Highly radiogenic and variable $^{187}\text{Os}/^{188}\text{Os}$ of Rožany ores at low $^{187}\text{Re}/^{188}\text{Os}$ (Fig. 9a) can be best explained by either osmium addition or rhenium removal lowering original $^{187}\text{Re}/^{188}\text{Os}$. The former possibility is highly unlikely as Rožany dolerites penetrate the Lusatian Granitoid Complex with granitic composition, which should contain very little Os preventing some significant Os addition via late-stage remobilization from the host rock. In comparison, several studies have shown that Re can be highly mobile during hydrothermal alteration (Walker et al. 1994, 2007) or dehydration (Becker 2000). Taking into account several observations described above giving the clear evidence for late-stage hydrothermal alteration, variable Re loss is the most viable explanation for the observed Re–Os compositions of the Rožany ores.

5.3. Comparison with other Ni–Cu–(PGE) mineralizations of the Bohemian Massif

In the Bohemian Massif, three occurrences of Ni–Cu–(PGE) mineralizations have been described so far. They are located in the Variscan Ransko gabbro–peridotite massif (e.g., Misař 1974; Pašava et al. 2003; Ackerman et al. 2013), the Svitavy ultramafic complex (e.g., Kopecký 1992; Pašava et al. 2007) and Kunratice–Rožany dolerites (Pašava et al. 2001; this study). All these mineralizations are characterized by the strong predominance of P-PGE over I-PGE at high, but variable Pd/Pt ratios of 1.4 to 36, which is typical of magmatic–hydrothermal PGE deposits associated with base-metal sulphides (pyrrhotite, pentlandite and chalcopyrite). Analysed massive and disseminated ores from Rožany have total PGE contents of 0.15–0.20 g/t which is similar to Svitavy (Pašava et al. 2007), but much lower than Ransko where the richest samples yield almost 1 g/t (Pašava et al. 2003). The differences between the Ransko and Rožany–Kunratice mineralizations can be also recognized in the presence of different PGM. At Ransko, the PGE mineralization is bound to PtAs₂ (sperrylite), PdBiTe (michenerite) and PdBi₂ (froidite). In comparison, the Rožany–Kunratice PGE mineralization is characterized by the presence of Pt–As and Pt–Te (moncheite) as the main Pt carriers, whereas Pd is bound to Pd–Bi–Te and Pd–Ni–Bi–Te phases (this study and Pašava et al. 2001). These differences most likely reflect distinct source of Variscan parental magmas (primitive tholeiitic melts at Ransko and enriched alkaline intraplate melts in the Lusatian Granitoid Complex – Abdelfadil et al. 2013) and melt differentiation.

6. Conclusions

The Ni–Cu–(PGE) mineralization at Rožany (northern Czech Republic) is hosted by dolerite dykes cross-cutting Lusatian Granitoid Complex of Cadomian age. New *in-situ* LA-ICP-MS U–Pb zircon data for Rožany dolerite yield an age of 349 ± 3 Ma, which is much lower than previous K–Ar and Pb–Pb ages of ~ 400 Ma. The reason for this discrepancy is most likely the observed presence of inherited zircon cores and/or zircon recrystallization/partial dissolution during late-stage hydrothermal processes. Trace-element and Re–Os isotopic composition of barren dolerites suggest derivation of the parental magmas from enriched (metasomatized) mantle source possibly related to subduction processes. The Ni–Cu–(PGE) mineralization is represented by pyrrhotite, pentlandite and chalcopyrite formed as magmatic sulphides by the separation of sulphur-saturated melts at the final stages of parental melt differentiation. Common presence of violarite seems to be connected with hydrothermal alteration of pentlandite. Detected Pd- and Pt-bearing platinum-group minerals (PGM) are enclosed not only in all identified base-metal sulphides, but also in rock-forming silicate minerals and their alteration products (e.g., chlorite) indicating that formation of at least some of the PGM was closely associated with late-stage hydrothermal remobilization from the primary base-metal sulphides and/or their enclosed PGM. The I-PGE (Os–Ir–Ru) are concentrated in Ni-rich ores whereas Pd and Pt tend to be predominantly concentrated in Cu-rich ores forming their own PGM. All types of massive and disseminated ores show highly variable γ Os (349 Ma) values from +50 to +134 contrasting with nearly constant $^{187}\text{Re}/^{188}\text{Os}$ values. This can be best explained by combination of variable incorporation of crustal material to parental melt and post-crystallization modification of Re–Os systematics by hydrothermal processes leading to removal of rhenium. In comparison to the Ransko Ni–Cu–(PGE) mineralization, the Rožany locality is characterized by much lower platinum-group element contents. The difference in identified PGM is slight, though, as the main PGE-carriers in Rožany–Kunratice are also Pt–As, Pt(Pd)–Te, Pd–Bi–Te and Pd–Ni–Te phases.

Acknowledgements. This work represents the contribution to the project of the Czech Science Foundation (no. 13-15390S to L.A. and J.P.). We are indebted to Patricie Týcová for taking cathodoluminescence images of zircon, Jana Ďurišová for the help with zircon U–Pb analyses, Vojtěch Erban for maintaining of TIMS lab in the Czech Geological Survey and to Zdeňka Lhničková for analyses of sulphur isotopes. The research project of Institute of Geology of the Czech Academy of Sciences RVO67985831 is also acknowledged. Two anonymous

reviewers are thanked for their careful reading of the manuscript leading to improvement of the text. Final corrections and suggestions by Editor-in-Chief Vojtěch Janoušek are highly appreciated.

References

- ABDEFADIL KM, ROMER RL, SEIFERT T, LOBST R (2013) Calc-alkaline lamprophyres from Lusatia (Germany) – evidence for a repeatedly enriched mantle source. *Chem Geol* 353: 230–245
- ACKERMAN L, PAŠAVA J, ERBAN V (2013) Re–Os geochemistry and geochronology of the Ransko gabbro–peridotite massif, Bohemian Massif. *Miner Depos* 48: 799–804
- BECKER H (2000) Re–Os fractionation in eclogites and blueschists and the implications for recycling of oceanic crust into the mantle. *Earth Planet Sci Lett* 177: 287–300
- BERNARD JH (1991) Empirical Types of Ore Mineralizations in the Bohemian Massif. Czech Geological Survey, Prague, pp 1–181
- BIALEK D, KRYSZA R, OBERC-DZIEDZIC T, PIN C (2014) Cambrian Zawidów granodiorites in the Cadomian Lusatian Massif (Central European Variscides): what do the SHRIMP zircon ages mean? *J Geosci* 59: 313–326
- BIRCK JL, BARMAN MR, CAPMAS F (1997) Re–Os isotopic measurements at the femtomole level in natural samples. *Geostand Geoanal Res* 20: 19–27
- BORKOWSKA M, HAMEURT I, VIDAL P (1980) Origin and age of Isera-gneisses and Rumburk-granites in the Western Sudetes. *Acta Geol Pol* 30: 121–144
- CAWTHORN R, MERKLE RKW, VILJOEN MJ (2002) Platinum-group elements deposit in the Bushveld Complex, South Africa. In: CABRI LJ (ed) *The Geology, Geochemistry, Mineralogy and Mineral Beneficiation of Platinum-group Elements*. Canadian Institute of Mining, Metallurgy and Petroleum, Montreal, pp 389–430
- CHÁB J, BREITER K, FATKA O, HLADIL J, KALVODA J, ŠIMŮNEK Z, ŠTORCH P, VAŠÍČEK Z, ZAJÍC J, ZAPLETAL J (2010) Outline of the Geology of the Bohemian Massif. Czech Geological Survey, Prague, pp 1–284
- COHEN AS, WATERS FG (1996) Separation of osmium from geological materials by solvent extraction for analysis by thermal ionisation mass spectrometry. *Anal Chim Acta* 332: 269–275
- CREASER RA, PAPANASTASSIOU DA, WASSERBURG GJ (1991) Negative thermal ion mass spectrometry of osmium, rhenium, and iridium. *Geochim Cosmochim Acta* 55: 397–401
- CROCKET JH (2002) Platinum-group element geochemistry of mafic and ultramafic rocks. In: CABRI LJ (ed) *The Geology, Geochemistry, Mineralogy and Mineral Beneficiation of Platinum-group Elements*. Canadian Institute of Mining, Metallurgy and Petroleum, Montreal, pp 177–210
- DALE CW, LUGUET A, MACPHERSON CG, PEARSON DG, HICKEY-VARGAS R (2008) Extreme platinum-group element fractionation and variable Os isotope compositions in Philippine Sea Plate basalts: tracing mantle source heterogeneity. *Chem Geol* 248: 213–238
- DÖRR W, ZULAUF G, FIALA J, FRANKE W, VEJNAR Z (2002) Neoproterozoic to Early Cambrian history of an active plate margin in the Teplá–Barrandian unit – a correlation of U–Pb isotopic-dilution-TIMS ages (Bohemia, Czech Republic). *Tectonophysics* 352: 65–85
- ESSER BK, TUREKIAN KK (1993) The osmium isotopic composition of the continental crust. *Geochim Cosmochim Acta* 57: 3093–3104
- FARROW CEG, LIGHTFOOT PC (2002) Sudbury PGE Revisited: toward an integrated model. In: CABRI LJ (ed) *The Geology, Geochemistry, Mineralogy and Mineral Beneficiation of Platinum-group Elements*. Canadian Institute of Mining, Metallurgy and Petroleum, Montreal, pp 273–297
- GODEL B, BARNES SJ, MAIER WD (2007) Platinum-group elements in sulphide minerals, platinum-group minerals, and whole-rocks of the Merensky Reef (Bushveld Complex, South Africa): implications for the formation of the reef. *J Petrol* 48: 1569–1604
- GOTTLIEB P, WILKIE G, SUTHERLAND D, HO-TUN E, SUTHERS S, PERERA K, JENKINS B, SPENCER S, BUTCHER A, RAYNER J (2000) Using quantitative electron microscopy for process mineralogy applications. *JOM* 52: 24–25
- GRGURIC BA (2002) Hypogene violarite of exsolution origin from Mount Keith, Western Australia: field evidence for a stable pentlandite–violarite tie line. *Mineral Mag* 66: 313–326
- GRINENKO VA (1962) The preparation of sulphur dioxide for isotopic analysis. *Zhurnal Neorg Khimii* 7: 478–483
- HOSKIN PWO, SCHALTEGGER U (2003) The composition of zircon and igneous and metamorphic petrogenesis. In: HANCHAR JM, HOSKIN PWO (eds) *Zircon*. Mineralogical Society of America Reviews in Mineralogy and Geochemistry 53, pp 27–62
- ISHIKAWA A, SENDA R, SUZUKI K, DALE CW, MEISEL T (2014) Re-evaluating digestion methods for highly siderophile element and ¹⁸⁷Os isotope analysis: evidence from geological reference materials. *Chem Geol* 384: 27–46
- JACKSON SE, PEARSON NJ, GRIFFIN WL, BELOUSOVA EA (2004) The application of laser ablation-inductively coupled plasma-mass spectrometry to in situ U–Pb zircon geochronology. *Chem Geol* 211: 47–69
- KINDERMANN A, FIEDLER F, SEIFERT T, UHLIG S (2003) Platinmetall-Führung der Ni–Cu–Sulfidmineralisationen im Bereich der Lausitzer Antiklinalzone. *Z Angew Geol* 49: 43–47
- KOMAROVA MZ, KOZYREV SM, SIMONOV ON, LULKO VA (2002) The PGE mineralization of disseminated sulphide ores of the Noril'sk–Taimyr region. In: CABRI LJ (ed)

- The Geology, Geochemistry, Mineralogy and Mineral Beneficiation of Platinum-group Elements. Canadian Institute of Mining, Metallurgy and Petroleum, Montreal, pp 547–567
- KOOIJMAN E, BERNDT J, MEZGER K (2012) U–Pb dating of zircon by laser ablation ICP-MS: recent improvements and new insights. *Eur J Mineral* 24: 5–21
- KOPECKÝ L (1992) Perspectives of Ni–Cu (Pt), Cr mineralizations of the subcretaceous basic and ultramafic complex near Svitavy. *Věst Čes Geol Úst* 67: 245–257
- KOSMATT F (1927) Gliederung des variszischen Gebirgsbaues. *Abh Sächs Geol Landesamts* 1: 1–39
- KOZDRÓJ W, KRENTZ O, OPLETAL M (2001) Geological map Lausitz–Jizera–Karkonosze (without Cenozoic sediments), scale 1: 100 000. Czech Geological Survey, Prague
- KRAMER W (1977) Zur tektonischen und substantiellen Charakteristik der Basite des Lausitzer Antiklinoriums und deren Altersbeziehungen. *Z Geol Wiss* 5: 95–100
- KRÖNER A, HEGNER E, HAMMER J, HAASE G, BIELICKI KH, KRAUSS M, EIDAM J (1994) Geochronology and Nd–Sr systematics of Lusatian granitoids – significance for the evolution of the Variscan orogen in east-central Europe. *Geol Rundsch* 83: 357–376
- KYLINDER-CLARK ARC, HACKER BR, COTTLE JM (2013) Laser-ablation split-stream ICP petrochronology. *Chem Geol* 345: 99–112
- LESHER CM, ARNDT NT, GROVES DI (1984) Genesis of komatiite-associated nickel sulphide deposits at Kambalda, Western Australia: a distal volcanic model. In: BUCHANAN DL, JONES MJ (eds) *Sulphide Deposits in Mafic and Ultramafic Rocks*. Institution of Mining and Metallurgy, London, pp 70–80
- LIGHTFOOT PC, DOHERTY W (2001) Chemical evolution and origin of nickel sulphide mineralization in the Sudbury Igneous Complex, Ontario, Canada. *Econ Geol* 96: 1855–1875
- LINNEMANN U, GEHMLICH M, TICHOMIROVA M, BUSCHMANN B, NASDALA L, JONAS P, LÜTZNER H, BOMBACH K (2000) From Cadomian subduction to Early Palaeozoic rifting: the evolution of Saxo-Thuringia at the margin of Gondwana in the light of single zircon geochronology and basin development (Central European Variscides, Germany). In: FRANKE W, HAAK V, ONCKEN O, TANNER D (eds) *Orogenic Processes: Quantification and Modelling in the Variscan Belt*. Geological Society Special Publications 179, London, pp 131–153
- LINNEMANN U, MCNAUGHTON NJ, ROMER RL, GEHMLICH M, DROST K, TONK C (2004) West African provenance for Saxo-Thuringia (Bohemian Massif): did Armorica ever leave pre-Pangean Gondwana? U/Pb-SHRIMP zircon evidence and the Nd-isotopic record. *Int J Earth Sci* 93: 683–705
- LINNEMANN U, GERDES A, DROST K, BUSCHMANN B (2007) The continuum between Cadomian orogenesis and opening of the Rheic Ocean: constraints from LA-ICP-MS U–Pb zircon dating and analysis of plate-tectonic setting (Saxo-Thuringian zone, NE Bohemian Massif, Germany). In: LINNEMANN U, NANCE RD, KRAFT P, ZULAUFG (eds) *The Evolution of the Rheic Ocean: From Avalonian–Cadomian Active Margin to Alleghenian–Variscan Collision*. Geological Society of America Special Papers 423, pp 61–96
- LINNEMANN U, D'LEMONS R, DROST K, JEFFRIES T, GERDES A, ROMER RL, SAMSON SD, STRACHAN RA (2008) Cadomian tectonics. In: MCCANN T (ed) *The Geology of Central Europe – Volume 1, Precambrian and Paleozoic*. Geological Society of London, London, pp 103–154
- MATTE P (2001) The Variscan collage and orogeny (480–290 Ma) and the tectonic definition of the Armorica microplate: a review. *Terra Nova* 13: 122–128
- MCDONOUGH WF, SUN S (1995) The composition of the Earth. *Chem Geol* 120: 223–253
- MERLET C (1994) An accurate computer correction program for quantitative electron-probe microanalyses. *Microchim Acta* 114: 363–376
- MORGAN JW, WALKER RJ, HORAN MF, BEARY ES, NALDRETT AJ (2002) ^{190}Pt – ^{186}Os and ^{187}Re – ^{187}Os systematics of the Sudbury Igneous Complex, Ontario. *Geochim Cosmochim Acta* 66: 273–290
- MÍSAŘ Z (1974) *The Ransko Gabbro–Peridotite Massif*. Charles University, Prague, pp 1–215
- NALDRETT AJ (2010) *Magmatic Sulfide Deposits*. Springer-Verlag, Berlin–Heidelberg, pp 1–727
- OBERC-DZIEDZIC T, KRYZA R, PIN C, MOCHNACKA K, LARIONOV A (2009) The Orthogneiss and Schist Complex of the Karkonosze–Izera Massif (Sudetes, SW Poland): U–Pb SHRIMP zircon ages, Nd-isotope systematics and protoliths. *Geol Sudetica* 41: 3–24
- OBERC-DZIEDZIC T, KRYZA R, MOCHNACKA K, LARIONOV A (2010) Ordovician passive continental margin magmatism in the Central-European Variscides: U–Pb zircon data from the SE part of the Karkonosze–Izera Massif, Sudetes, SW Poland. *Int J Earth Sci* 99: 27–46
- PAŠAVA J, VAVŘÍN I, JELÍNEK E (2001) Distribution of PGE in rocks and Ni–Cu ores of the Rožany and Kunratice deposits (Lusatian Massif, Bohemian Massif). In: PIESTRZYŃSKI A (ed) *Mineral Deposits at the Beginning of the 21st Century*. Proceedings of the Joint 6th Biennial SGA–SEG Meeting. Balkema, Rotterdam–Krakow, pp 627–633
- PAŠAVA J, VAVŘÍN I, FRÝDA J, JANOUŠEK V, JELÍNEK E (2003) Geochemistry and mineralogy of platinum-group elements in the Ransko gabbro–peridotite massif, Bohemian Massif (Czech Republic). *Miner Depos* 38: 298–311
- PAŠAVA J, VYMAZALOVÁ A, KNĚSL I, ACKERMAN L (2007) PGE in ultramafic rocks of the hidden ophiolite complex near Svitavy, Bohemian Massif. In: ANDREW CJ (ed) *Digging Deeper Proceedings of 9th Biennial SGA Meeting*, Dublin. Balkema, Rotterdam–Krakow, pp 1591–1594

- PATON C, HELLSTROM J, PAUL B, WOODHEAD J, HERGT J (2011) Iolite: freeware for the visualisation and processing of mass spectrometric data. *J Anal Atom Spec* 26: 2508–2518
- PETRUS JA, KAMBER BS (2012) VizualAge: A novel approach to laser ablation ICP-MS U–Pb geochronology data reduction. *Geostand Geoanal Res* 36: 247–270
- PEUCKER-EHRENBRINK B, JAHN B (2001) Rhenium–osmium isotope systematics and platinum group element concentrations: loess and the upper continental crust. *Geochem Geophys Geosys* 2: 1061, DOI: 10.1029/2001gc000172
- POKORNÝ J (1969) Sulphide ore deposits in the Ransko basic massif. *Sbor geol Věd, Ložisk Geol Mineral* 10: 111–154
- RIPLEY EM, LI C (2003) Sulfur isotope exchange and metal enrichment in the formation of magmatic Cu–Ni (PGE) deposits. *Econ Geol* 98: 635–641
- SCHULMANN K, KONOPÁSEK J, JANOUŠEK V, LEXA O, LARDEAUX J-M, EDEL J-B, ŠTÍPSKÁ P, ULRICH S (2009) An Andean type Palaeozoic convergence in the Bohemian Massif. *C R Geosci* 341: 266–286
- SHIREY SB, WALKER RJ (1995) Carius tube digestion for low-blank rhenium–osmium analyses. *Anal Chim Acta* 67: 2136–2141
- SHIREY SB, WALKER RJ (1998) The Re–Os isotope system in cosmochemistry and high-temperature geochemistry. *Annu Rev Earth Planet Sci* 26: 423–500
- SMITH AJB, VILJOEN KS, SCHOUWSTRA R, ROBERTS J, SCHALKWYK C, GUTZMER J (2013) Geological variations in the Merensky Reef at Bafokeng Rasimone platinum mine and its influence on flotation performance. *Miner Eng* 52: 155–168
- TENAILLEAU C, PRING A, ETSCHMANN B, BRUGGER J, GRGURIC B, PUTNIS A (2006) Transformation of pentlandite to violarite under mild hydrothermal conditions. *Amer Miner* 91: 706–709
- TICHOMIROVA M (2002) Zircon inheritance in diatexite granodiorites and its consequence on geochronology – a case study in Lusatia and the Erzgebirge (Saxo-Thuringia, eastern Germany). *Chem Geol* 191: 209–224
- VAVŘÍN I, FRÝDA J (1998) Pd–Pt–As–Te mineralization from the Kunratic and Rožany copper–nickel deposits of Šluknov area. *Věst Čes Geol Úst* 73: 177–180 (in Czech)
- VÖLKENING J, WALCZYK T, HEUMANN KG (1991) Osmium isotope ratio determinations by negative thermal ionization mass spectrometry. *Int J Mass Spectrom Ion Process* 105: 147–159
- WALKER RJ, MORGAN JW, HANSKI E, SMOLKIN VF (1994) The role of the Re–Os isotopic system in deciphering the origin of magmatic sulphide ores: a tale of three ores. In: LIGHTFOOT PC, NALDRETT AJ (eds) *Proceedings of Sudbury–Norilsk Symposium*. Ontario Geological Survey, Toronto, pp 343–355
- WALKER RJ, BOHLKE C, McDONOUGH WF, LI J (2007) Effects of mother lode-type gold mineralization on $^{187}\text{Os}/^{188}\text{Os}$ and platinum group element concentrations in peridotite: Alleghany District, California. *Econ Geol* 102: 1079–1089
- WIEDENBECK M, ALLÉ P, CORFU F, GRIFFIN WL, MEIER M, OBERLI F, VON QUADT A, RODDICK JC, SPIEGEL W (1995) Three natural zircon standards for U–Th–Pb, Lu–Hf, trace element and REE analyses. *Geostand Geoanal Res* 19: 1–23
- ŽELAŽNIEWICZ A, FANNING CM, ACHRAMOWICZ S (2009) Refining the granite, gneiss and schist interrelationships within the Lusatian–Izera Massif, West Sudetes, using SHRIMP U–Pb zircon analyses and new geologic data. *Geol Sudetica* 41: 67–84